The role of the tryptophan-nicotinamide pathway in a model of severe malnutrition induced liver dysfunction

Guanlan Hu [1,2], Catriona Ling [1,2], Lijun Chi [2], Samuel Furse [3], Albert Koulman [3], Jonathan Swann [4,5], Mehakpreet K. Thind [1,2], Dorothy Lee [2], Marjolein Calon [2], Christian J. Versloot [6], Barbara M. Bakker [6], Gerard B. Gonzales [2,7,8], Peter K. Kim [9,10] & Robert H.J. Bandsma [1,2,11,12] *

[1] Department of Nutritional Sciences, Faculty of Medicine, University of Toronto, Toronto, ON M5G 1A8, Canada

[2] Translational Medicine Program, The Hospital for Sick Children, Toronto, ON M5G 0A4, Canada

[3] Core Metabolomics and Lipidomics Laboratory, Wellcome Trust-Metabolic Research Laboratories, Institute of Metabolic Sciences, University of Cambridge, Cambridge, CB2 0QQ, United Kingdom

[4] School of Human Development and Health, Faculty of Medicine, University of Southampton, SO16 6YD, United Kingdom

[5] Department of Metabolism, Digestion and Reproduction, Faculty of Medicine, Imperial College London, SW7 2AZ, United Kingdom

[6] Laboratory of Pediatrics, Center for Liver, Digestive, and Metabolic Diseases, University of Groningen, University Medical Center Groningen, Groningen, The Netherlands

[7] Gastroenterology, Department of Pediatrics and Internal Medicine, Faculty of Medicine and Health Sciences, Ghent University, Ghent 9000, Belgium

[8] VIB Inflammation Research Center, Zwijnaarde 9052, Belgium

[9] Department of Biochemistry, University of Toronto, Toronto, ON M5S 1A8, Canada

[10] Cell Biology Program, The Hospital for Sick Children, Toronto, ON M5G 0A4, Canada

[11] Division of Gastroenterology, Hepatology, and Nutrition, The Hospital for Sick Children, Toronto, ON M5G 0A4, Canada

[12] The Childhood Acute Illness & Nutrition Network (CHAIN), Blantyre, Malawi

* Correspondence and requests for materials should be addressed to

Robert H.J. Bandsma, Translational Medicine Program, The Hospital for Sick Children, Peter Gilgan Centre for Research and Learning, 686 Bay Street, Toronto, ON M5G 0A4, Canada. Tel.: +1 4168137654x9057; Fax: +1 4168134972 (R.H.J. Bandsma).

E-mail address: robert.bandsma@sickkids.ca (R.H.J. Bandsma)

Abstract

Mortality in children with severe malnutrition is strongly related to signs of metabolic dysfunction, such as hypoglycemia. Lower circulating tryptophan levels in children with severe malnutrition suggest a possible disturbance in the tryptophan-nicotinamide (TRP-NAM) pathway and subsequently NAD+ dependent metabolism regulator sirtuin1 (SIRT1). We report that severe malnutrition in weanling mice, induced by feeding a low protein diet, leads to an impaired TRP-NAM pathway and affects hepatic mitochondrial turnover and function. We demonstrate that stimulating the TRP-NAM pathway improves hepatic mitochondrial and overall metabolic function which is dependent on SIRT1. Activating SIRT1 is sufficient to induce improvement in metabolic functions. Our findings indicate that modulating the TRP-NAM pathway can partially improve liver metabolic function in severe malnutrition and could lead to the development of new interventions for children with severe malnutrition.

Introduction

Malnutrition contributes to nearly 45% of deaths among children under 5 years of age worldwide[1]. Malnourished children, especially those with severe malnutrition are at a substantially increased risk of mortality compared to well-nourished children[2]. The current treatment guidelines developed by the World Health Organization (WHO) for children with severe malnutrition are based on limited scientific evidence[3]. Thus, new evidence-based interventions are urgently needed.

The liver is a central organ that regulates nutrient metabolism. In severe malnutrition, hepatic metabolism has been found to be disturbed and is associated with hypoglycemia, hypoalbuminemia, and steatosis[4-6]. Children with severe malnutrition have impaired hepatic glucose production, which increases the risk of hypoglycemia and is related to mortality[5]. We recently discovered in both patients and a rodent model of severe malnutrition, that hepatic mitochondrial function is impaired leading to reduced nutrient oxidation and adenosine triphosphate (ATP) depletion[5,6]. However, the pathophysiology of hepatic mitochondrial dysfunction in severe malnutrition remains poorly understood.

Children with severe malnutrition have been found to have significantly lower serum tryptophan levels[7-9]. As an essential amino acid, tryptophan is crucial for growth and protein synthesis. It is also a precursor of nicotinamide adenine dinucleotide (NAD+) and nicotinamide adenine dinucleotide phosphate (NADP+), which are essential co-factors in metabolic and biosynthesis pathways. We have previously shown that higher excretion of *N*-methylnicotinamide, a urinary biomarker of NAD+ and nicotinamide availability, was associated with catch-up growth in stunted infants[10]. NAD+ is also a co-substrate for sirtuin1 (SIRT1), which is an important enzyme for mitochondrial health and biogenesis through activation of peroxisome proliferator-activated receptor-gamma coactivator-1 alpha (PGC-1α)[11]. SIRT1 has also been shown to regulate autophagy[12-14]. There have been reports that targeting this pathway in non-alcoholic fatty liver disease (NAFLD) has beneficial effects on hepatic metabolism[15-18]. The role of tryptophan nicotinamide (TRP-NAM) pathway in severe malnutrition-associated hepatic metabolic dysfunction remains unknown.

In this study we aimed to characterize the role of the TRP-NAM pathway in hepatic metabolic dysfunction in a mouse model of severe malnutrition. We demonstrate that the TRP-NAM pathway is affected in this model and that hepatic mitochondrial dysfunction is related to deficiencies in the TRP-NAM pathway. We demonstrate supplementing with NAM and related components of this pathway improve mitochondrial and overall hepatic metabolic dysfunction. We find that the effects of modulating the TRP-NAM pathway are mediated through SIRT1. These findings identify the importance of the TRP-NAM pathway and SIRT1 in malnutrition-associated hepatic metabolic dysfunction.

Results

Feeding a low protein diet leads to hepatic steatosis in young mice.

To develop a mouse model of severe malnutrition, we fed 3-weeks-old weanling male C57BL/6J mice a 1% protein isocaloric diet for two weeks (malnourished group) and compared it to the control group fed an 18% protein diet (control group) (Fig. 1a). Mice subjected to the 1% protein diet lost a significant amount of body weight (approximately 20%) over two weeks and had a lower body length and weight for length ratio compared to the 18% protein-fed control group (Fig. 1b-d). The 1% protein-fed mice showed a lower liver weight and liver to body weight ratio compared to control (Fig. 1e). Lower glucose concentrations were also noted in the 1% protein-fed mice before and after fasting (Fig. 1f), consistent with reduced hepatic glucose production. The respiratory exchange ratio (RER) was lower during the dark phase and higher during the light phase in 1% protein-fed mice, indicating a loss of the day-night feeding cycle in this group. Energy expenditure was lower in 1% protein-fed mice compared to the 18% protein-fed control group (Fig. 1g).

Histological H&E staining and Oil Red O staining of the livers identified steatosis in the mice fed with 1% protein diet as evidenced by an increase in fat vacuoles and larger fat droplets compared to the mice fed with 18% protein diet (Fig 2a-b). The increase in lipid droplets in the liver of the 1% protein-fed mice was confirmed by immunofluorescence staining with BODIPY (Fig. 2c). Further quantification of histology slides showed consistency with these observations (Fig. 2d)

and was validated by measurement of liver triglyceride (TG) levels (Fig. 2e). Serum TGs were lower in the 1% protein-fed group, indicating steatosis is not linked to hypertriglyceridemia (Fig. 2f). Together, these results indicate that the 1% protein diet induces hepatic steatosis in mice similar to those observed in patients and rat model of severe malnutrition[2,6].

NAM and TRP-NAM pathway modulators reduce the development of low protein diet-induced hepatic steatosis.

Examination for blood tryptophan levels showed the 1% protein diet mice to be lower than 18% protein diet control animals (43.0±5.0 μmol/L and 88.4±13.2 μmol/L respectively, p=0.0035). To examine the role of a reduced tryptophan levels and possible nicotinamide (NAM) deficiency on liver health, the 1% protein-fed mice were supplemented with 160 mg/kg body weight NAM from day 7 to day 14 (Fig. 1a). NAM treatment did not alter the average body weight, body length, or food and liquid consumption in the 1% protein-fed group (Fig. 1b-d). The mice treated with NAM had no significant difference in liver weight, liver/body weight ratio, or fasting glucose levels compared to the untreated 1% protein diet-fed mice (Fig. 1e-f). RER and energy expenditure were not affected by NAM treatment (Fig. 1g). NAM treatment improved the hepatic steatosis compared to the 1% protein-fed mice, indicated by a reduction in the fat vacuoles area and a 30% reduction in liver TG levels compared to untreated animals (Fig. 2a-e). The NAM treatment had no effect on serum TG concentrations (Fig. 2f).

To determine whether the effect of NAM treatment was due to improvement of the NAD salvage pathway specifically, we treated the 1% protein-fed mice with nicotinamide riboside (NR) or tryptophan (TRP). Both NR and TRP act as NAD+ precursors in the NAD salvage pathway[16]. The allocated interventions were given from day 7 to day 14 (Supplementary Fig. 1a). NR and TRP supplementation, similar to NAM treatment, did not recover body weight, body length or liver weight/body weight ratio compared to the untreated 1% protein-fed group (Supplementary Fig. 1b-e). Similar to the NAM treated malnourished mice, hepatic steatosis was reduced in the NR and TRP treated groups (Supplementary Fig. 2a-f). To determine whether the effects were specific to the TRP-NAM pathway, we also performed similar experiments in mice who received supplementation with methionine (MET), another essential amino acid like tryptophan. This

particular amino acid was chosen as MET has been shown to decrease hepatic steatosis in mice on ketogenic diets[19], and diets completely devoid of MET and choline can induce hepatic steatosis[20,21]. Supplementation with methionine did not improve hepatic steatosis among the 1% protein-fed mice (Supplementary Fig. 2a-f). MET supplementation also did not recover body weight and body length, but increased liver weight and body weight ratio in comparison to the untreated 1% protein-fed mice alone (Supplementary Fig. 1b-d). Together, these results indicate that supplementation of different NAD+ precursors improve low protein-induced hepatic steatosis.

NAM improves low protein diet-induced mitochondrial changes.

To further understand the mechanisms underlying the improved hepatic steatosis in response to NAM treatment, we next evaluated changes in hepatic mitochondrial characteristics in our model. We have previously shown that protein-deficient diet induces mitochondrial morphological and functional changes and reduces mitochondrial activity in rats under protein restricted diet[6]. In our mouse model, immunofluorescent staining of mitochondria in the liver showed that the mitochondria were enlarged and elongated but decreased in numbers in the 1% protein-fed mice compared to the 18% protein-fed control group (Fig. 3a). The loss of mitochondria was further confirmed by a significant decrease in the mitochondrial DNA (mtDNA) copy number (Fig. 3b). This feature improved after NAM, NR, and TRP treatment (Fig. 3b, Supplementary Fig. 2h). Mitochondrial abundance markers including TOM20 and HSP60 were both significantly lower in the 1% protein diet-fed mice compared to the control, but improved with NAM treatment (Fig. 3c,d). This suggests that NAM treatment can either reduce mitochondria degradation or increase its biogenesis in our model of severe malnutrition.

To examine mitochondrial fitness, we examined hepatic ATP levels, and levels of mitochondrial complex proteins. Further, we quantified the expression of genes in the β-oxidation and lipogenesis pathway. The livers of the 1% protein-fed malnourished mice had significantly lower hepatic ATP levels compared to the 18% protein-fed control group (Fig. 3e). NAM and other TRP-NAM pathway modulators significantly restored hepatic ATP levels (Fig. 3e, Supplementary Fig. 2i). Complex I, Complex IV, and Complex V protein levels were significantly lower in the 1% protein-fed group compared to the control group (Fig. 3f,g). Complex IV levels improved significantly

after NAM treatment, while no significant change was observed in levels of other complexes. Expression of the genes in the β-oxidation pathway was reduced in the livers of mice fed a 1% protein diet and were partially restored after NAM treatment, especially Acaa2 and Hadha (Fig. 3h). The expression of lipogenesis genes including Fasn and Acaca were decreased in mice fed a 1% protein diet (Fig. 3i). NAM supplementation did not influence the mRNA expression of lipogenesis genes (Fig. 3i). In summary, feeding mice a 1% protein diet altered the hepatic mitochondrial morphology, decreased mitochondrial number and mass, and affected markers of oxidative phosphorylation and β-oxidation. NAM treatment improved the 1% protein diet-induced mitochondrial changes associated with a recovery in ATP content.

A low protein diet leads to changes in hepatic energy metabolism that improve with NAM treatment.

To better understand the overall liver metabolic change in mice fed with 1% protein diet and evaluate the effect of NAM supplementation, we performed quantitative analysis of liver central carbon metabolism metabolites[22]. The major metabolic profile differences between groups was highlighted by sparse-partial least squares-discriminant analysis (sPLS-DA)[23]. Variable importance in projection (VIP) scores were used to identify the most important metabolites for the clustering. Overall, the hepatic metabolic profiles of the 1% protein diet-fed malnourished group were clearly separated from those of the 18% protein diet-fed control group, and distinct from NAM treatment group (Fig. 4a-b). Among the metabolomic features, acetylglucosamine-1P, glycerylaldehyde-3P, malonyl-CoA, lactic acid, ATP, erythrose-4P, UMP, UDP-glucose, glucose, pyruvic acid, and ADP-glucose mostly discriminated 18% protein diet from 1% protein diet groups, with variable importance in projection (VIP) score >1 in both components 1 and 2 (Fig. 4a). To be more specific, the 1% protein-fed group showed significantly lower glucose, lactic acid, and pyruvic acid content compared to control (Supplementary Table 1)[24]. GMP and UMP concentrations decreased in the 1% protein diet-fed group, suggesting disturbed nucleotide metabolism including pyrimidine and purine synthesis. Malonyl-CoA levels also changed in the 1% protein-diet fed group, consistent with altered lipogenesis[25,26]. The overall results were also in line with an earlier report of impaired ATP production and decreased pyruvate uptake,

accompanied by altered tricarboxylic acid cycle (TCA) cycle intermediates in a rat model of malnutrition[6]. Modulation of the TRP-NAM pathway altered hepatic metabolic profiles as observed by sPLS-DA (Fig. 4b and Supplementary Fig. 3a). NAM treatment shifted malonyl-CoA, UTP, ATP, Hs-CoA, UDP-Glucose, total fructose-bisP/glucose-1,6-bisP, acetyl-CoA, AMP, and succinyl-CoA, which mostly differentiate them with 1% protein diet group (VIP score >1). The concentration of ATP, malonyl-CoA, and acetyl-CoA in NAM treated group shifted towards the 18% protein diet-fed control group, which was related to the improved energy production and carbohydrate and lipid metabolism (Supplementary Table 1)[27].

To further explore the changes in lipid metabolism in our model and evaluate the effect of TRP-NAM modulation, we performed a lipidomic analyses. Overall, discriminating features were identified that clearly separate the 18% protein diet and 1% protein diet group, dominated by increased levels of triacylglycerols, diacylglycerols, and sterols (VIP score >1) (Fig. 4c and Supplementary Table 2). Interestingly, hepatic phospholipid content was lower in the 1% group compared to the 18% group. The decreased PC/TG ratio and phosphatidylcholines to phosphatidylethanolamines ratio (PC/PE) in the 1% protein diet group might be linked to the altered energy metabolism and lipid droplet size and dynamics[28,29]. Decreased PC/PE ratios have also been observed in NASH patients[30,31], potentially through mitochondrial respiratory chain dysfunction and disability to meet energy requirements[32]. NAM treatment clearly separated this group from the 1% protein diet group and separation was primarily caused differences in phosphatidylcholines and diacylglycerols (VIP score >1) (Fig. 4d and Supplementary Table 2). NR and TRP treatment groups were close to each other but clearly separate from MET treatment group, mostly highlighted by altered triacylglycerols and diacylglycerols (with VIP score >1) (Supplementary Fig. 3b).

NAM treatment affects NAD+ and the SIRT1 pathway in low protein-fed mice.

To determine whether NAM treatment directly affects the NAD salvage pathway, we measured the abundance of hepatic NAD+ and tryptophan pathway metabolites in the liver of these animals. NAD+ levels and many metabolites in the tryptophan pathway (such as kynurenine, kynurenine acid, serotonin) were decreased in the 1% protein-fed mice compared to the 18% protein-fed

control group (Fig. 5a). NAM treatment increased hepatic nicotinic acid concentrations, indicating NAM was bioavailable and affected the TRP-NAM pathway. However, we did not observe a significant effect of NAM treatment on NAD+ levels itself ($p = 0.640$), whereas NR treatment did significantly increase hepatic NAD+ levels (Supplementary Fig. 2j). This result is consistent with other studies that have reported that NR increased hepatic NAD+ levels[33]. Another chronic NAM supplementation study showed that NAM did not boost NAD+ but enhanced the de-acetylation of SIRT1 targets[18].

Next, we investigated changes in the NAD dependent SIRT1 pathway. The protein levels of SIRT1 and its downstream target PGC-1α were significantly decreased in the mice fed a 1% protein diet compared to the 18% protein-fed control group and levels of these proteins were significantly improved after NAM treatment, albeit not to the same level as the control group (Fig. 5b,e). The ratio of p65 to Ac-p65 significantly increased in the 1% protein-fed group compared to the control, which was improved after NAM treatment, indicating a change in SIRT1 deacetylation activity (Fig. 5c,e).

Since SIRT1 has been shown to influence autophagy and we previously showed an impairment in autophagy flux in livers of low protein-fed rodents[6], we next evaluated autophagy levels by measuring microtubule-associated protein 1A/1B-light chain 3 (LC3) LC3-I and LC3-II protein levels. Autophagy pathway marker of LC3-II/LC3-I ratio significantly decreased in the 1% protein-fed malnourished group compared to the 18% protein-fed control group, suggesting a decrease in autophagy activation (Fig. 5d,e). NAM treatment increased the LC3-II/LC3-I ratio, which suggests an increase in activation of macro-autophagy. Taken together, our results suggest that the TRP-NAM pathway is disturbed after feeding a 1% protein diet to mice and that it can be partially restored by NAM treatment. In turn, the improvement in the TRP-NAM pathway elevates SIRT1 which may be linked to the increase in PGC-1α and activation of autophagy.

The effect of NAM on low protein diet-induced liver metabolic dysfunction is mediated through SIRT1.

To further test the whether the effect of NAM is SIRT1-dependent, we performed experiments using SIRT1 modulators in the 1% protein-fed mice with or without NAM supplementation (Fig. 6a). The SIRT1 activator, resveratrol (REV)[34,35], was used to investigate if SIRT1 activation was sufficient to demonstrate an improvement in the hepatic metabolic changes caused by 1% protein feeding. The SIRT1 inhibitor, selisistat (EX-527)[36,37], was subsequently used in combination with NAM treatment to determine if the effect of NAM was dependent on the activation of SIRT1.

Intraperitoneal injection of REV did not change body weight, body length and liver weight compared to the vehicle control group (Fig. 6b-e). However, we observed a decrease in the degree of hepatic steatosis in the 1% protein-fed malnourished group treated with REV, with nearly 2 folds decrease in fat vacuole area and decreased liver TG levels compared to untreated 1% protein fed animals (Fig. 7a,b). mtDNA copy number and ATP levels significantly increased after REV treatment (Fig. 7c,d). Among the β-oxidation genes, we observed small but significant increases in Hadha and Acadm expression after REV treatment, without a significant change in expression of lipogenesis genes compared to vehicle treated group (Fig. 7e,f). When the 1% protein-fed malnourished mice were treated with both EX-527 and NAM, the effects of NAM treatment on hepatic steatosis and mtDNA copy number were lost (Fig. 7a-c). SIRT1 protein level was upregulated after REV treatment (Fig. 7g). There was also a trend toward increased PGC-1α protein levels in the REV treated group (p-value = 0.083). EX-527 with NAM treatment also did not affect SIRT1 and PGC-1α levels compared to the 1% protein-fed malnourished group alone (Fig. 7g). These data indicate that the SIRT1 increase is sufficient to improve 1% protein diet-induced hepatic metabolic dysfunction and the effect of NAM treatment on hepatic metabolism is dependent on the elevation of SIRT1.

Discussion

Our study indicates that feeding weanling mice a 1% protein diet leads to stunted growth, severe wasting, hepatic lipid accumulation and mitochondrial dysfunction that is associated with a reduction in activity in SIRT1, PGC-1α and autophagy. We demonstrate that supplementing the TRP-NAM pathway is able to improve the metabolic phenotype and that this effect is dependent

on SIRT1. This is the first report on the role of the TRP-NAM pathway in a murine malnutrition model.

The hepatic metabolic changes induced by the protein deficient diet were consistent with our previous findings in a rat model of severe malnutrition showing liver steatosis and ATP depletion caused by mitochondrial dysfunction in a rat model of severe malnutrition[11]. The data are also consistent with limited reports in children with severe malnutrition that have found impaired mitochondrial function[4,5]. Interestingly, there is considerable overlap with features seen in patients with NAFLD, including changes in mitochondrial complexes, mitochondrial biogenesis, and hepatic lipid accumulation[38-40]. The reduction in mitochondrial mass seen in our mouse model is different from previous observations in low protein fed rats, where an increase in mitochondrial mass was observed[6]. However, reduction in mtDNA in our low protein diet mouse model was consistent with another previous report in fetal and early postnatal malnourished rats fed a low casein diet[41].

The reduction in mitochondrial mass and mtDNA in low protein-fed mice was associated with a reduction in PGC-1α, a well-known regulator of cellular energy metabolism and activator of mitochondrial biogenesis[42,43]. PGC-1α can co-activate transcription factors such as peroxisome proliferator-activated receptor (PPARα) and nuclear respiratory factors (NRF1 and NRF2) to regulate mitochondrial biogenesis and fatty acid oxidation[44]. Mice that are deficient in PGC-1α have impaired energy metabolism that is related to a decrease in mitochondrial number and respiratory capacity[45]. This suggests that the reduction in mitochondrial mass is related to a decrease in mitochondrial biogenesis upon low protein feeding. The changes in mitochondrial morphology, mitochondrial complex content, and markers of mitochondrial function, such as ATP, also indicate that the mitochondria that are present in the liver after a period of low protein feeding are damaged and dysfunctional. Mitochondrial degradation is regulated through a selective autophagy process called mitophagy[12], and our data suggests that autophagy activation is decreased during nutritional stress. This could contribute to a high relative content of damaged mitochondria that would normally have been degraded through mitophagy. NAM treatment increased PGC-1α protein levels, mitochondrial mass and content of mitochondrial complexes, while activating the autophagy pathway, suggesting a rebalancing of mitochondrial biogenesis and mitophagy.

PGC-1α and autophagy are both regulated by SIRT1. SIRT1 directly deacetylates PGC-1α at multiple lysine sites and the induction pattern of SIRT1 protein correlates with the expression of PGC-1α[46]. In addition, SIRT1 regulate autophagy by acting on multiple autophagy effectors. These mechanisms include directly inducing autophagy by deacetylating autophagy-related genes (ATGs) and LC3, indirectly inhibiting the mTOR pathway by activation of AMPK, as well as modulating the expression of autophagy and mitophagy regulatory molecules (e.g. Rab7 and Bnip3) through deacetylation of Forkhead box O transcription factors (FOXOs)[47,48]. SIRT1 levels were decreased in our low protein diet-fed mice. As SIRT1 activity is dependent on NAD availability, we propose that lower SIRT1 activity is associated with reduced levels of NAD and other metabolites in the TRP-NAM pathway in low protein diet-fed mice. Supplementing these protein deficient animals with NAM was found to rescue SIRT1 mediated activity. We propose that the reduction in NAD prevents the SIRT1 mediated activation of PGC-1α and autophagy pathway. Our results are consistent with a clinical study reporting that increased malnutrition risk was associated with decreased SIRT1 expression[49]. The decreased protein levels of SIRT1 found after low protein feeding could potentially be explained by diet-triggered cleavage of SIRT1 protein. For example, a high-fat diet has been shown to induce SIRT1 protein cleavage leading to metabolic dysfunction[50].

NAM was shown to increase SIRT1 levels. The effect was not specific to NAM, as NR and TRP demonstrated a similar effect. Other NAD+ precursors such as NR and TRP have demonstrated a similar effect in previous studies[17,51,52]. We focused on NAM specifically for more in depth investigations because of its low cost and excellent safety profile. Treatment with NAM and other NAD+ precursors have shown beneficial effects in various metabolic dysfunction models, including fatty liver, obesity, metabolic syndrome, and diabetes[18,53,54]. The beneficial effects in these studies have been related to an improved mitochondrial function, mediated by NAD+ dependent sirtuin activation[17,51,52]. Our SIRT1 modulation experiments demonstrated that in our malnutrition model the effects of NAM were dependent on the presence of SIRT1 and that stimulating SIRT1 was sufficient to produce the beneficial effects on mitochondrial function. The results are consistent with studies in high fat-fed mice where resveratrol impacted mitochondrial function and prevented hepatic steatosis[34].

In our study, NAM treatment did not significantly restore NAD+ levels whereas NR did, however NAM improved SIRT1 and PGC-1α levels. Some studies have shown that NAM has the ability to increase cellular and blood NAD+ content in different metabolic disorder models (*e.g.* NAFLD mice, hepatocytes with endoplasmic reticulum stress)[55-58]. However, other studies have found no direct effect of NAM supplementation on NAD+ levels[18,59]. If the extra NAD that is synthesized, is readily used for deacetylation, then you would not see a significant increase. These differences in findings might also be related to the duration and variation in the dose of NAM and the animal models used affecting NAM metabolism. For example, NAM can affect SIRT1 activity differently by acting as a non-competitive end-product inhibitor and as a NAD+ precursor[60]. In addition, NAM clearance pathways through MNAM-mediated SIRT1 protein stabilization can also regulate hepatic nutrient metabolism[61,62].

In conclusion, this work provides evidence for the role of TRP-NAM pathway in liver metabolic dysfunction in a mouse model of severe malnutrition, mediated through changes in levels of SIRT1. This study improves our understanding of the cellular pathophysiology of severe malnutrition. The results of this project could lead to the development of new interventions that target the TRP-NAM pathway which could then be taken to clinical trials.

Methods

Animals and diets. A breeding colony of C57BL/6 mice was obtained from Jackson Laboratories (Bar Harbor, ME, USA). Male mice at 3 weeks post-partum were weaned and housed socially in filtered cages at The Hospital for Sick Children, Toronto. Weanling male C57BL/6J mice were randomized into different groups fed with control diet (18% protein) or malnourished diet (1% protein) for a period of 2 weeks. Diets were purchased from ENVIGO (Madison, WI, USA), and the protein proportions contribute to diet calories were primarily adjusted by casein and corn starch. After 7 days, malnourished subgroups were treated with modulators of the TRP-NAM pathway until sacrifice on day 14. Nicotinamide, nicotinamide-riboside and tryptophan were given by drinking water in a dose of 160 mg/kg body weight/day, and methionine was included in diets at a concentration of 0.75 g/kg diet[15,59,63]. Nicotinamide, nicotinamide-riboside and tryptophan

were provided by Sigma-Aldrich (St. Louis, MO, USA). In a subset of mice, after 1% protein diet for 7 days, intraperitoneal injections treated with either resveratrol (25 mg/kg/d) or EX-527 (10 mg/kg/d) with NAM were given for 7 consecutive days until sacrifice[36,37,64]. All groups were housed in a temperature-controlled environment (23 °C), 12 h light-dark cycle, and had ad libitum access to diet and water throughout the study. All animal experiments were approved by the Animal Care Committee of The Hospital for Sick Children, Toronto (Animal Use Protocol Number: 1000030900).

Physiological parameters. Body weight, food intake, and liquid intake were monitored from day 1 to day 14. At the end of the experimental protocol (on day 14 post weaning), mice were humanely euthanized and necropsied. Final body weight, body length, and liver weight were recorded. Blood was collected by cardiac puncture. Liver tissue was collected for histology or stored at -80 °C for later use in biochemical analyses. Glucose concentration was determined via tail snip at 0h, 4h, 8h, and 12h fasting in the day light cycle, using an automatic glucometer (Freestyle, Abbott, IL). Metabolic rate was assessed by indirect calorimetry using the Columbus Instruments (Oxymax Lab Animal Monitoring System: CLAMS, Columbus, OH)[18].

Histology. Fresh livers tissues were fixed in 4% paraformaldehyde (PFA) overnight at 4 °C and then embedded in either paraffin or optimum cutting temperature (OCT) compound. Liver paraffin sections (5 μm) were stained with hematoxylin and eosin (H&E) for morphology. Liver OCT sections were stained with Oil red O (10 μm) for lipid droplets. Slides were visualized under a light microscope and was measured using Panoramic Viewer version 1.15 software (3DHISTECH Ltd, Budapest, Hungary). For each slide, at least five pictures were captured. Quantification analysis of the images was conducted using ImageJ 1.52v and Python 3.7.2.

Immunofluorescence. OCT-embedded liver sections were cut into 4 μm slices for immunofluorescent staining. A fluorinated boron-dipyrromethene (BODYPI) antibody was used to visualize fat droplets. An HSP60 antibody was used to visualize mitochondrial morphology. Nuclei were counterstained with DAPI. Slides were mounted with mounting medium (Vector Laboratories Inc., Burlington, Canada) and images were acquired on a Nikon Spinning Disk Confocal Microscope (Nikon Inc., NY, USA). Additional information can be found in the Supplementary Table 3.

Plasma tryptophan analysis. Plasma samples were mixed with equal volumes of internal standard (Norleucine). Samples were centrifuged at 14000 rpm for 5 minutes and subsequently measured on Biochrom 30+ Amino Acid Analyzer (Biochrom, Cambridge, UK).

Triglyceride analysis. Liver and serum TG concentrations were quantified by a commercially available kit (Randox, London, UK). Liver tissue lipids were extracted with methanol-chloroform, dried and dissolved for TG analysis. Values were also normalized to protein concentrations determined using a bicinchoninic acid assay (BCA) kit (Thermo Fisher Scientific, USA).

Western blotting. Western blot analysis was conducted to measure the protein levels. Liver tissue protein was extracted through sonication of tissue with extraction buffer and protease inhibitor cocktail (Sigma-Aldrich). The protein concentration was measured using pierce BCA kit (Thermo Fisher Scientific). Equal concentrations of the samples were electrophoresed through 4%-12% Bis Tris gel and transferred onto a polyvinylidene fluoride (PVDF) membrane. Membranes were probed with 1:1000 dilutions of anti HSP60 (Abcam, USA), TOM20 (Santa Cruz, USA), Complex I (Abcam, USA), Complex IV (Abcam, USA), Complex V (Abcam, USA), SIRT1 (Cell Signalling, USA), PGC-1α (Abcam, USA), p65 (Abcam, USA), Ac-p65 (Abcam, USA), LC3B (Sigma, USA). β-actin (Sigma, USA) was used as a loading control in 1:1000 dilution. Then proteins were visualized using a pierce enhanced chemiluminescence (ECL) plus kit (Invitrogen, CA, USA). Western blot quantification was performed using Image Studio (LI-COR Biosciences). Additional information can be found in the Supplementary Table 3.

qPCR. Total RNA was isolated from frozen liver tissue using Direct-zol RNA MiniPrep Kit (ZYMO research Inc., Irvine, CA, USA). cDNA was synthesized by the Super Script VILO cDNA Synthesis Kit (Thermo Fisher Scientific, USA). 500 ng of liver total RNA were used for cDNA synthesis. Ribosomal protein l13a (Rpl13a) was used as reference gene. qPCR was performed on CFX384 Touch Real-Time PCR Detection System (Bio-Rad, CA, USA). For mtDNA copy number measurements, 500 ng of genomic DNA were used for each qPCR reaction and β-globin were used as reference[65]. Additional information can be found in the Supplementary Table 4.

Metabolomic analysis. Targeted metabolomic profiling (pathway specific assays) was performed by The Metabolomics Innovation Centre (TMIC, Edmonton, AB Canada). The quantitation of central carbon metabolism metabolites in mouse liver was measured by ultraperformance liquid

chromatography-tandem mass spectrometry (UPLC-MS/MS). A Dionex 3400 UHPLC system coupled to a 4000 QTRAP mass spectrometer was used. The MS instrument was operated in the multiple-reaction monitoring (MRM) mode with negative-ion (-) or positive-ion (+) detection, depending on which groups of metabolites were measured. Each liver tissue sample was frozen and placed into an Eppendorf tube. Water, at 2 μL per mg tissue, was added and the samples were homogenized for 1 min twice at a shaking frequency of 30 Hz, with the aid of two 4-mm metal balls, on a MM 400 mill mixer. After a short-time centrifuge, methanol, at 8 μL per mg tissue, was added and the samples were homogenized again for 1 min twice using the same settings. The samples were then sonicated in an ice-water bath for 3 min, followed by centrifugal clarification at 15,000 rpm and 5 °C in an Eppendorf 5424R centrifuge for 20 min. The clear supernatants were collected to conduct quantitation of TCA cycle carboxylic acids, glucose and selected sugar phosphates, and other phosphate-containing metabolites and nucleotides by UPLC-MS/MS. Concentrations of the detected metabolites were calculated from their linear-regression calibration curves with internal calibration. Tryptophan pathway metabolites were also measured using a UPLC-MS based targeted method[66].

Lipidomic analysis. Lipidomic analysis was performed at Core Metabolomics and Lipidomics Laboratory, Wellcome Trust-Metabolic Research Laboratories (University of Cambridge, Cambridge, UK). Liver samples were homogenised, lipids were extracted according to a published procedure, and data was acquired through Direct Infusion Mass Spectrometry (DI-MS)[67]. Briefly, liver sections (30 mg/each) were homogenised (Tissue homogeniser II, Qiagen) in a buffer of chaeotropes (guanidinium chloride (6 M) and thiourea (1.5 M) in deionised water, 500 μL/sample). The liver homogenates (30 μL) were injected into a well (96w plate, Esslab Plate+™, 2.4 mL/well, glass-coated) followed by methanol spiked with internal standards (150 μL), water (500 μL) and DMT (500 μL, dichloromethane, methanol and triethylammonium chloride, 3:1:0.005). Most of the aqueous solution was removed (96 channel pipette). A portion of the organic solution (20 μL) was transferred to a high throughput plate (384 w, glass coated, Esslab Plate+™) before being dried (N_2 (g)). The dried films were re-dissolved (TBME, 30 μL/well) and diluted with a stock mixture of alcohols and ammonium acetate (100 μL/well; propan-2-ol: methanol, 2:1; CH_3COONH_4 7.5 mM). The analytical plate was heat-sealed and run immediately. Lipid fraction isolates were profiled using a three-part method in DI-MS[67]. All samples were infused into an Exactive Orbitrap (Thermo, Hemel Hampstead, UK), using a TriVersa NanoMate (Advion, Ithaca

US). Samples (15 µL) were sprayed at 1.2 kV in the positive ion mode. The Exactive started acquiring data 20 s after sample aspiration began. The Exactive acquired data with a scan rate of 1 Hz (resulting in a mass resolution of 100,000 full width at half-maximum [fwhm] at 400 *m/z*). The Automatic Gain Control was set to 3,000,000 and the maximum ion injection time to 50 ms. After 72 s of acquisition in positive mode the NanoMate and the Exactive switched over to negative ionization mode, decreasing the voltage to -1.5 kV and the maximum ion injection time to 50 ms. The spray was maintained for another 66 s, after which the NanoMate and Exactive switched over to negative mode with in-source fragmentation (also known as collision-induced dissociation, CID; 70 eV) for a further 66 s. After this time, the spray was stopped and the tip discarded, before the analysis of the next sample began. The sample plate was kept at 15 °C throughout the acquisition. Samples were run in row order. The instrument was operated in full scan mode from *m/z* 150-1200 Da (for singly charged species).

Statistical analysis. Statistical significance for the difference between two groups was calculated by using an unpaired two-tailed student's T-test. Statistical significance for the difference among more than two groups was calculated by using an ordinary one-way ANOVA followed by the Turkey's post hoc test[68]. The FDR and Bonferroni correction were applied to the metabolomic and lipidomic metabolites. Statistical analysis was performed with R software (version 3.5.2) and MetaboAnalyst (version 4.0). Statistical significance was given as * $p < 0.05$, ** $p < 0.01$, and *** $p < 0.001$. The results are expressed as mean ± standard error of mean (S.E.M.), unless otherwise indicated.

Data availability

All relevant data of this study are available within the paper and its supplementary information files. All data that support this study are available from the corresponding authors upon reasonable request.

References

1. WHO. Children: reducing mortality. World Health Organization: WHO. http://www.who.int/news-room/fact-sheets/detail/children-reducing-mortality (2019).
2. Bhutta, Z.A., *et al.* Severe childhood malnutrition. *Nat Rev Dis Primers* **3**, 17067 (2017).
3. Guideline, W. Updates on the management of severe acute malnutrition in infants and children. *Geneva: World Health Organization* **2013**, 6-54 (2013).
4. McLean, A. Hepatic failure in malnutrition. *Lancet*, 1292-1294 (1962).
5. Bandsma, R.H., *et al.* Mechanisms behind decreased endogenous glucose production in malnourished children. *Pediatric research* **68**, 423 (2010).
6. van Zutphen, T., *et al.* Malnutrition-associated liver steatosis and ATP depletion is caused by peroxisomal and mitochondrial dysfunction. *J Hepatol* **65**, 1198-1208 (2016).
7. Di Giovanni, V., *et al.* Metabolomic changes in serum of children with different clinical diagnoses of malnutrition. *The Journal of nutrition* **146**, 2436-2444 (2016).
8. Tessema, M., *et al.* Associations among high-quality protein and energy intake, serum transthyretin, serum amino acids and linear growth of children in Ethiopia. *Nutrients* **10**, 1776 (2018).
9. Moreau, G.B., *et al.* Childhood growth and neurocognition are associated with distinct sets of metabolites. *EBioMedicine* **44**, 597-606 (2019).
10. Mayneris-Perxachs, J., *et al.* Urinary N-methylnicotinamide and beta-aminoisobutyric acid predict catch-up growth in undernourished Brazilian children. *Sci Rep* **6**, 19780 (2016).
11. Aquilano, K., *et al.* Peroxisome proliferator-activated receptor gamma co-activator 1alpha (PGC-1alpha) and sirtuin 1 (SIRT1) reside in mitochondria: possible direct function in mitochondrial biogenesis. *J Biol Chem* **285**, 21590-21599 (2010).
12. Jang, S.-y., Kang, H.T. & Hwang, E.S. Nicotinamide-induced mitophagy event mediated by high NAD+/NADH ratio and SIRT1 protein activation. *Journal of Biological Chemistry* **287**, 19304-19314 (2012).
13. Shen, C., *et al.* Nicotinamide protects hepatocytes against palmitate-induced lipotoxicity via SIRT1-dependent autophagy induction. *Nutr Res* **40**, 40-47 (2017).
14. Kang, H.T. & Hwang, E.S. Nicotinamide enhances mitochondria quality through autophagy activation in human cells. *Aging Cell* **8**, 426-438 (2009).
15. Gual, P. & Postic, C. Therapeutic potential of nicotinamide adenine dinucleotide for nonalcoholic fatty liver disease. *Hepatology* **63**, 1074-1077 (2016).
16. Rajman, L., Chwalek, K. & Sinclair, D.A. Therapeutic potential of NAD-boosting molecules: the in vivo evidence. *Cell Metab* **27**, 529-547 (2018).
17. Gariani, K., *et al.* Eliciting the mitochondrial unfolded protein response by nicotinamide adenine dinucleotide repletion reverses fatty liver disease in mice. *Hepatology* **63**, 1190-1204 (2016).
18. Mitchell, S.J., *et al.* Nicotinamide improves aspects of healthspan, but not lifespan, in mice. *Cell Metab* **27**, 667-676 e664 (2018).
19. Pissios, P., *et al.* Methionine and choline regulate the metabolic phenotype of a ketogenic diet. *Molecular metabolism* **2**, 306-313 (2013).
20. Finkelstein, J.D., Martin, J.J. & Harris, B. Effect of nicotinamide on methionine metabolism in rat liver. *The Journal of nutrition* **118**, 829-833 (1988).
21. Komatsu, M., *et al.* NNMT activation can contribute to the development of fatty liver disease by modulating the NAD (+) metabolism. *Sci Rep* **8**, 8637 (2018).

22. Della Torre, S.*, et al.* Short-term fasting reveals amino acid metabolism as a major sex-discriminating factor in the liver. *Cell Metab* **28**, 256-267 e255 (2018).
23. Chang, H.*, et al.* Identification of key metabolic changes during liver fibrosis progression in rats using a urine and serum metabolomics approach. *Sci Rep* **7**, 11433 (2017).
24. Gray, L.R., Tompkins, S.C. & Taylor, E.B. Regulation of pyruvate metabolism and human disease. *Cellular and molecular life sciences* **71**, 2577-2604 (2014).
25. Bandyopadhyay, G.K., Joseph, G.Y., Ofrecio, J. & Olefsky, J.M. Increased malonyl-CoA levels in muscle from obese and type 2 diabetic subjects lead to decreased fatty acid oxidation and increased lipogenesis; thiazolidinedione treatment reverses these defects. *Diabetes* **55**, 2277-2285 (2006).
26. Rasmussen, B.B.*, et al.* Malonyl coenzyme A and the regulation of functional carnitine palmitoyltransferase-1 activity and fat oxidation in human skeletal muscle. *The Journal of clinical investigation* **110**, 1687-1693 (2002).
27. Avila, D.V.*, et al.* Dysregulation of hepatic cAMP levels via altered Pde4b expression plays a critical role in alcohol-induced steatosis. *The Journal of pathology* **240**, 96-107 (2016).
28. van der Veen, J.N.*, et al.* The critical role of phosphatidylcholine and phosphatidylethanolamine metabolism in health and disease. (Elsevier, 2017).
29. Eisinger, K.*, et al.* Lipidomic analysis of the liver from high-fat diet induced obese mice identifies changes in multiple lipid classes. *Experimental and molecular pathology* **97**, 37-43 (2014).
30. Puri, P.*, et al.* A lipidomic analysis of nonalcoholic fatty liver disease. *Hepatology* **46**, 1081-1090 (2007).
31. Li, Z.*, et al.* The ratio of phosphatidylcholine to phosphatidylethanolamine influences membrane integrity and steatohepatitis. *Cell metabolism* **3**, 321-331 (2006).
32. Ling, J., Chaba, T., Zhu, L.F., Jacobs, R.L. & Vance, D.E. Hepatic ratio of phosphatidylcholine to phosphatidylethanolamine predicts survival after partial hepatectomy in mice. *Hepatology* **55**, 1094-1102 (2012).
33. Trammell, S.A.*, et al.* Nicotinamide riboside is uniquely and orally bioavailable in mice and humans. *Nat Commun* **7**, 12948 (2016).
34. Lagouge, M.*, et al.* Resveratrol improves mitochondrial function and protects against metabolic disease by activating SIRT1 and PGC-1α. *Cell* **127**, 1109-1122 (2006).
35. Ding, S.*, et al.* Resveratrol and caloric restriction prevent hepatic steatosis by regulating SIRT1-autophagy pathway and alleviating endoplasmic reticulum stress in high-fat diet-fed rats. *PloS one* **12**, e0183541 (2017).
36. Huang, J.*, et al.* The SIRT1 inhibitor EX-527 suppresses mTOR activation and alleviates acute lung injury in mice with endotoxiemia. *Innate immunity* **23**, 678-686 (2017).
37. Yang, X.*, et al.* SIRT1 inhibition promotes atherosclerosis through impaired autophagy. *Oncotarget* **8**, 51447 (2017).
38. Brunt, E.M. Histological assessment of nonalcoholic fatty liver disease in adults and children. *Clin Liver Dis (Hoboken)* **1**, 108-111 (2012).
39. Lee, K.*, et al.* Hepatic mitochondrial defects in a mouse model of NAFLD are associated with increased degradation of oxidative phosphorylation subunits. *Molecular & Cellular Proteomics*, mcp. RA118. 000961 (2018).
40. Pérez-Carreras, M.*, et al.* Defective hepatic mitochondrial respiratory chain in patients with nonalcoholic steatohepatitis. *Hepatology* **38**, 999-1007 (2003).

41. Park, K.S., *et al.* Fetal and early postnatal protein malnutrition cause long-term changes in rat liver and muscle mitochondria. *The Journal of nutrition* **133**, 3085-3090 (2003).
42. Wu, Z., *et al.* Mechanisms controlling mitochondrial biogenesis and respiration through the thermogenic coactivator PGC-1. *Cell* **98**, 115-124 (1999).
43. Piccinin, E., Villani, G. & Moschetta, A. Metabolic aspects in NAFLD, NASH and hepatocellular carcinoma: the role of PGC1 coactivators. *Nature Reviews Gastroenterology & Hepatology* **16**, 160-174 (2019).
44. Scarpulla, R.C. Metabolic control of mitochondrial biogenesis through the PGC-1 family regulatory network. *Biochimica et Biophysica Acta (BBA)-Molecular Cell Research* **1813**, 1269-1278 (2011).
45. Leone, T.C., *et al.* PGC-1α deficiency causes multi-system energy metabolic derangements: muscle dysfunction, abnormal weight control and hepatic steatosis. *PLoS biology* **3**(2005).
46. Rodgers, J.T., *et al.* Nutrient control of glucose homeostasis through a complex of PGC-1α and SIRT1. *Nature* **434**, 113-118 (2005).
47. Lee, I.H., *et al.* A role for the NAD-dependent deacetylase Sirt1 in the regulation of autophagy. *Proc Natl Acad Sci U S A* **105**, 3374-3379 (2008).
48. Kitada, M., Ogura, Y. & Koya, D. Chapter 3 - Role of sirt1 as a regulator of autophagy. in *Autophagy: Cancer, Other Pathologies, Inflammation, Immunity, Infection, and Aging* (ed. Hayat, M.A.) 89-100 (Academic Press, San Diego, 2016).
49. El Assar, M., *et al.* Better nutritional status is positively associated with mRNA expression of SIRT1 in community-dwelling older adults in the Toledo Study for Healthy Aging. *J Nutr* **148**, 1408-1414 (2018).
50. Chalkiadaki, A. & Guarente, L. High-fat diet triggers inflammation-induced cleavage of SIRT1 in adipose tissue to promote metabolic dysfunction. *Cell metabolism* **16**, 180-188 (2012).
51. Wang, S., *et al.* Nicotinamide riboside attenuates alcohol induced liver injuries via activation of SirT1/PGC-1alpha/mitochondrial biosynthesis pathway. *Redox Biol* **17**, 89-98 (2018).
52. Ritze, Y., Bardos, G., Hubert, A., Bohle, M. & Bischoff, S.C. Effect of tryptophan supplementation on diet-induced non-alcoholic fatty liver disease in mice. *Br J Nutr* **112**, 1-7 (2014).
53. Morizono, S., *et al.* Nicotinamide, not N1 methylnicotinamide, ameliorates hepatic steatosis via NAD-depended sirtuin activation. *Journal of Hepatology* **68**, S350-S351 (2018).
54. Mejía, S.Á., *et al.* Nicotinamide prevents sweet beverage-induced hepatic steatosis in rats by regulating the G6PD, NADPH/NADP+ and GSH/GSSG ratios and reducing oxidative and inflammatory stress. *European journal of pharmacology* **818**, 499-507 (2018).
55. Li, J., *et al.* Nicotinamide ameliorates palmitate-induced ER stress in hepatocytes via cAMP/PKA/CREB pathway-dependent Sirt1 upregulation. *Biochimica et Biophysica Acta (BBA)-Molecular Cell Research* **1853**, 2929-2936 (2015).
56. Majamaa, K., Rusanen, H., Remes, A.M., Pyhtinen, J. & Hassinen, I.E. Increase of blood NAD+ and attenuation of lactacidemia during nicotinamide treatment of a patient with the MELAS syndrome. *Life sciences* **58**, 691-699 (1996).
57. Williams, P.A., *et al.* Vitamin B3 modulates mitochondrial vulnerability and prevents glaucoma in aged mice. *Science* **355**, 756-760 (2017).

58. Liu, D., Gharavi, R., Pitta, M., Gleichmann, M. & Mattson, M.P. Nicotinamide prevents NAD+ depletion and protects neurons against excitotoxicity and cerebral ischemia: NAD+ consumption by SIRT1 may endanger energetically compromised neurons. *Neuromolecular Med* **11**, 28-42 (2009).
59. Sambeat, A.*, et al.* Endogenous nicotinamide riboside metabolism protects against diet-induced liver damage. *Nat Commun* **10**, 4291 (2019).
60. Hwang, E.S. & Song, S.B. Nicotinamide is an inhibitor of SIRT1 in vitro, but can be a stimulator in cells. *Cell Mol Life Sci* **74**, 3347-3362 (2017).
61. Hong, S.*, et al.* Nicotinamide N-methyltransferase regulates hepatic nutrient metabolism through Sirt1 protein stabilization. *Nature medicine* **21**, 887 (2015).
62. Canto, C., Menzies, K.J. & Auwerx, J. NAD+ metabolism and the control of energy homeostasis: a balancing act between mitochondria and the nucleus. *Cell metabolism* **22**, 31-53 (2015).
63. Hashimoto, T.*, et al.* ACE2 links amino acid malnutrition to microbial ecology and intestinal inflammation. *Nature* **487**, 477-481 (2012).
64. Ma, S.*, et al.* SIRT1 activation by resveratrol alleviates cardiac dysfunction via mitochondrial regulation in diabetic cardiomyopathy mice. *Oxidative medicine and cellular longevity* **2017**(2017).
65. Rooney, J.P.*, et al.* PCR based determination of mitochondrial DNA copy number in multiple species. in *Mitochondrial Regulation* 23-38 (Springer, 2015).
66. Whiley, L.*, et al.* Ultrahigh-Performance liquid chromatography tandem mass spectrometry with electrospray ionization quantification of tryptophan metabolites and markers of gut health in serum and plasma - application to clinical and epidemiology cohorts. *Analytical chemistry* **91**, 5207-5216 (2019).
67. Furse, S.*, et al.* A high-throughput platform for detailed lipidomic analysis of a range of mouse and human tissues. *Analytical and Bioanalytical Chemistry*, 1-12 (2020).
68. Singh, R.*, et al.* Autophagy regulates lipid metabolism. *Nature* **458**, 1131 (2009).

Acknowledgements

We thank The Metabolomics Innovation Centre for performing targeted metabolomic assays, thank Lucy Wang and Ainsley Su-Williams for performing the experiments, and thank Bijun Wen, Celine Bourdon, and Amber Farooqui for help with statistical analyzing methods and animal use protocol update. This research was supported by the Bill & Melinda Gates Foundation.

Author contributions

R.H.J.B. and G.H. were primarily responsible for the study design. G.H. wrote the manuscript. G.H., C.L., L.C., S.F., J.S., M.K.T., D.L., M.C., C.J.V., and G.B.G. contributed to the conduction of lab experiments. G.H., L.C., S.F., and J.S. contributed to data analysis. P.K.K., A.K., and B.M.B. provided expertise, interpreted results, and commented on the manuscript. All authors contributed to editing of the manuscript. R.H.J.B. was responsible for the final content of the manuscript.

Competing interests

All participants declare no competing interests.

Additional information

Supplementary Information is available for this paper.

Correspondence and requests for materials should be addressed to R.H.J.B.

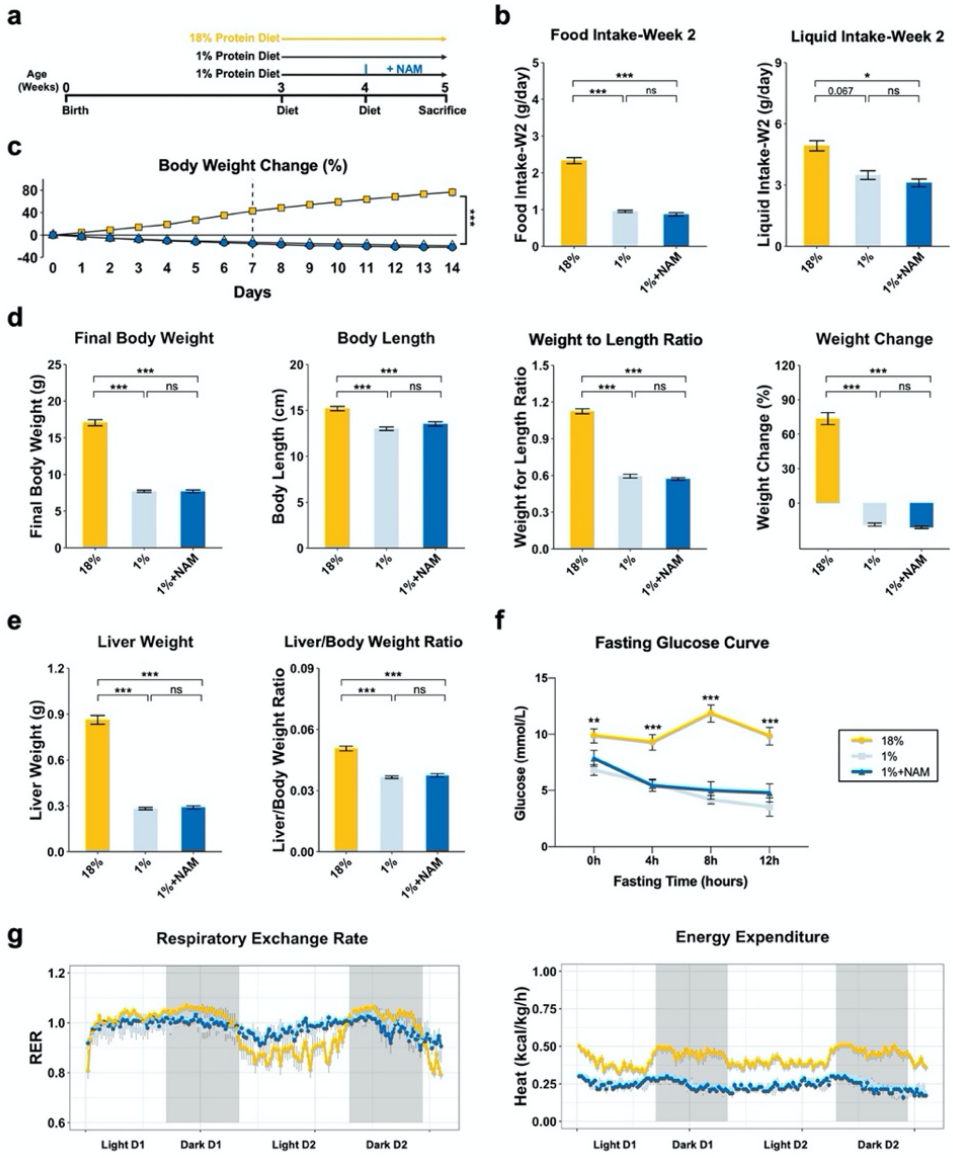

654

655 **Fig. 1 Feeding a 1% protein diet with or without NAM supplementation on basic animal**
656 **characteristics. a** Experimental design. **b** Average food and liquid intake during day 7 to day 14
657 (n=7 for 18%; n=5 for 1% and 1%+NAM). **c** Body weight change throughout experiment (n=15).
658 **d** Final body weight and body length assessed on day 14 (n=15). **e** Liver weight and liver
659 weight/body weight ratio (n=12 for 18%; n=10 for 1% and 1%+NAM). **f** Fasting glucose levels
660 (n=7 for 18%; n=8 for 1%; n=7 for 1%+NAM). **g** Respiratory exchange ratio (RER) and energy
661 expenditure (n=7 for 18%; n=6 for 1%; n=7 for 1%+NAM). $^{*}p < 0.05$, $^{**}p < 0.01$, $^{***}p < 0.001$, ns
662 as not significant, one-way ANOVA followed by Tukey's post hoc test. Data are shown as the
663 mean ± S.E.M.

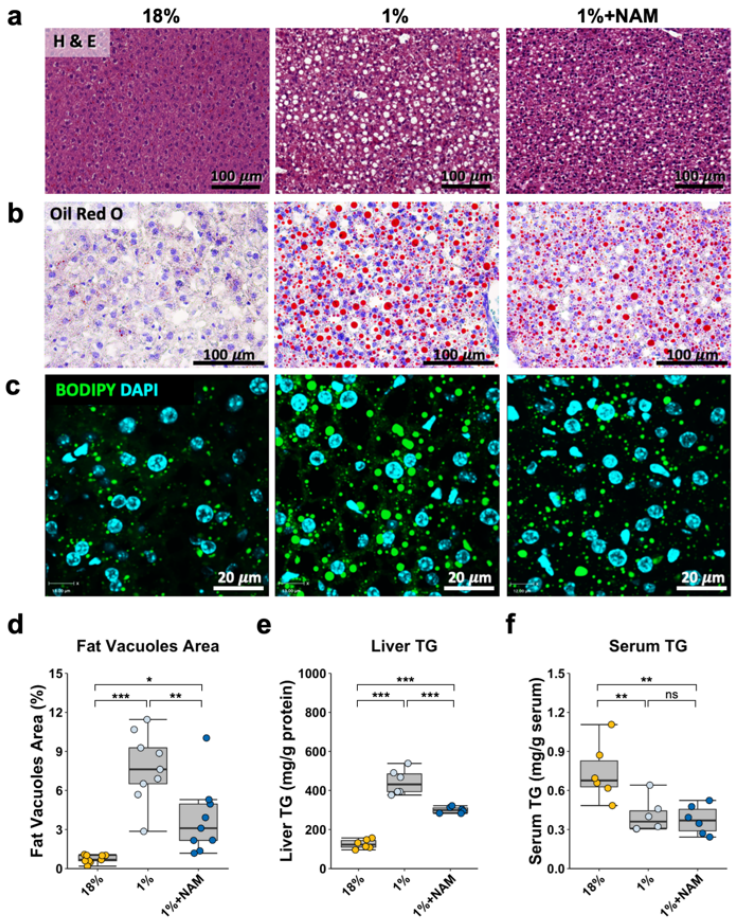

664

665 **Fig. 2 The effect of 1% protein feeding with or without NAM supplementation on hepatic**
666 **lipid accumulation. a** Representative hematoxylin and eosin staining images of the liver (20X
667 magnification). Cytoplasm was stained in red, and nucleus was stained in purple. **b** Representative
668 oil red o stain staining images of the liver (20X magnification). Fat droplet was stained in red, and
669 nucleus was stained in purple. **c** Representative immunofluorescence images of the liver (40X
670 magnification). BODYPY was used to stain fat droplet in green, and DAPI was used to counter
671 stain nucleus in blue. **d** Quantification of fat vacuoles area (n=9). **e** Liver TG concentrations (n=6).
672 **f** Serum TG concentrations (n=6). $^{*}p < 0.05$, $^{**}p < 0.01$, $^{***}p < 0.001$, ns as not significant, one-
673 way ANOVA followed by Tukey's post hoc test. Data are shown as the mean ± S.E.M. Scale bars
674 are as indicated.

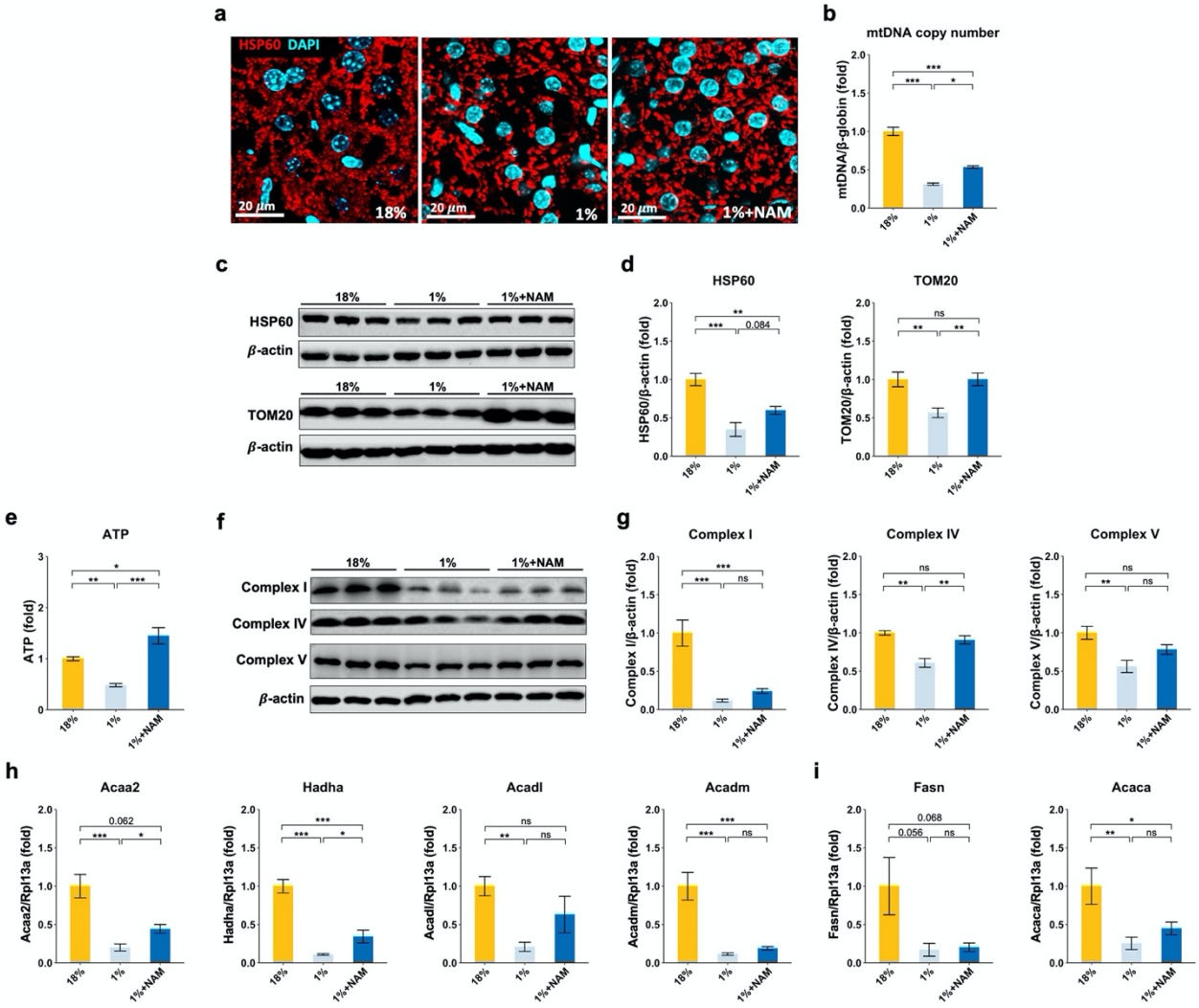

Fig. 3 The effect of NAM supplementation on mitochondrial characteristics of 1% protein fed model. a Representative immunofluorescence images of mitochondrial (60X magnification). HSP60 was used to stain mitochondrial in red, and DAPI was used to counter stain nucleus in blue. **b** mtDNA copy number (n=6). **c**, **d** Western blots and quantification of HSP60 and TOM20 (n=3). **e** ATP levels (n=11 for 18% and 1%; n=7 for 1%+NAM). **f, g** Western blots and quantification of complex I, complex IV and complex V (n=3). **h** mRNA expression of β-oxidation genes (n=6). **i** mRNA expression of lipid genesis genes (n=6). $^{*}p < 0.05$, $^{**}p < 0.01$, $^{***}p < 0.001$, ns as not significant, one-way ANOVA followed by Tukey's post hoc test. Data are shown as the mean ± S.E.M. Scale bars are as indicated.

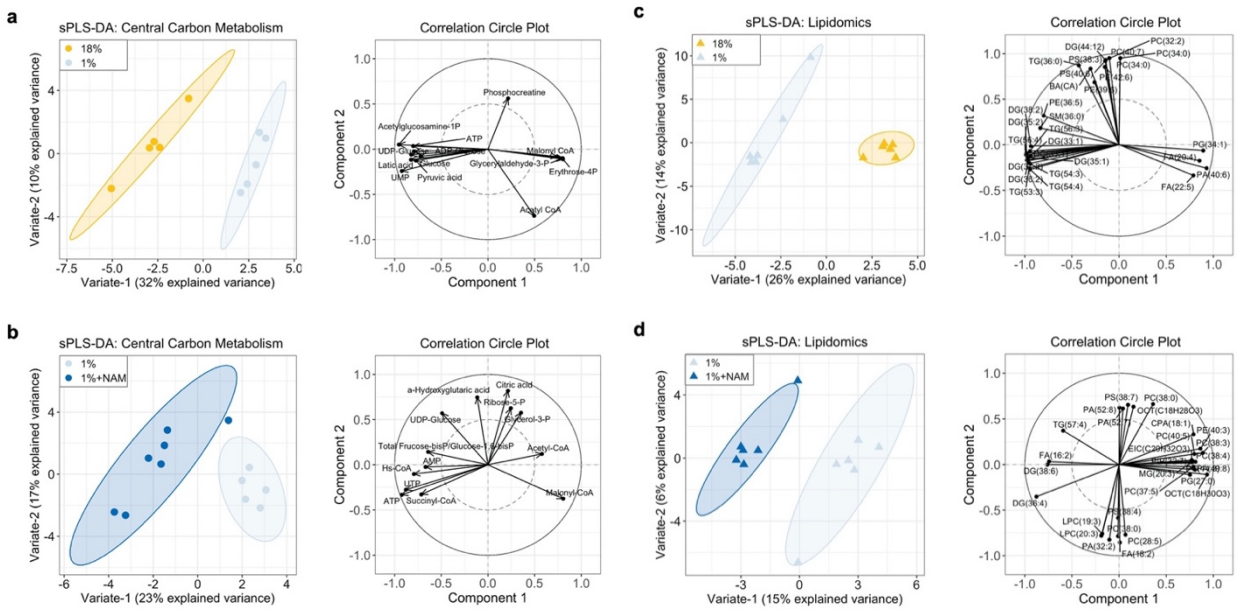

685

686 **Fig. 4 Hepatic metabolomic and lipidomic profiles under 18% protein diet, 1% protein diet,**
687 **and 1% protein diet with NAM supplementation. a** sPLS-DA and correlation circle plots of
688 hepatic central carbon metabolism showing separation of 18% and 1% protein diet group (n=5). **b**
689 sPLS-DA and correlation circle plots of hepatic central carbon metabolism showing separation of
690 1% protein diet and NAM treated group (n=5 for 1%; n=7 for 1%+NAM). **c** sPLS-DA and
691 correlation circle plots of hepatic lipidomics showing separation of 18% and 1% protein diet group
692 (n=6). **d** sPLS-DA and correlation circle plots of hepatic lipidomics showing separation of 1%
693 protein diet and NAM treated group (n=6).

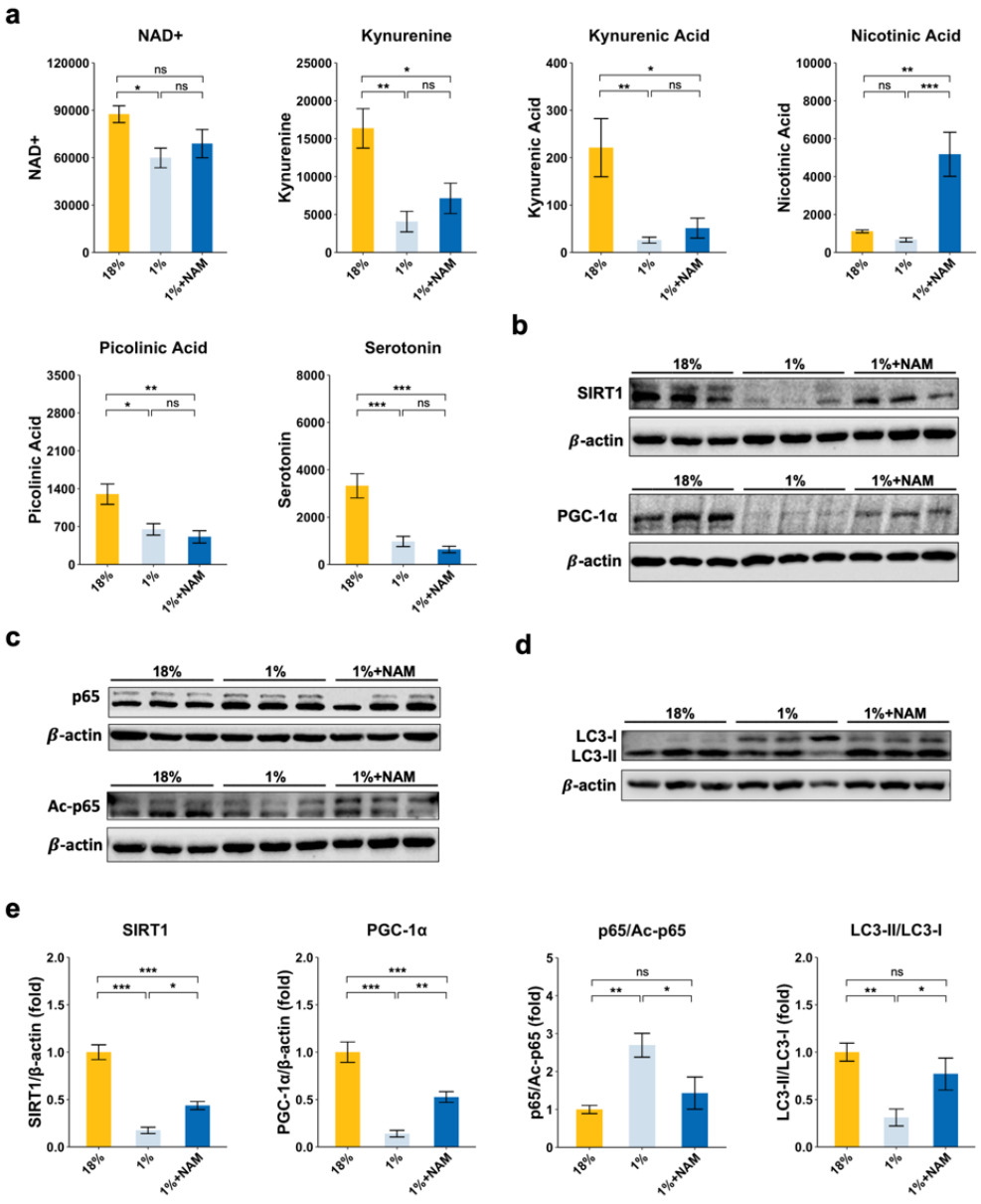

694

695 **Fig. 5 The effect of 1% protein feeding with or without NAM supplementation on TRP-NAM**
696 **pathway metabolites, SIRT1 and downstream targets, and autophagy levels. a** Hepatic NAD+
697 levels and TRP-NAM pathway metabolites (n=6). **b** SIRT1 and PGC-1α western blots (n=3). **c**
698 p65 and Acetyl-p65 western blots (n=3). **d** Autophagy markers LC3 western blots (n=3). **e**
699 Quantification of protein levels in western blots. $^{*}p < 0.05$, $^{**}p < 0.01$, $^{***}p < 0.001$, ns as not
700 significant, one-way ANOVA followed by Tukey's post hoc test. Data are shown as the mean ±
701 S.E.M.

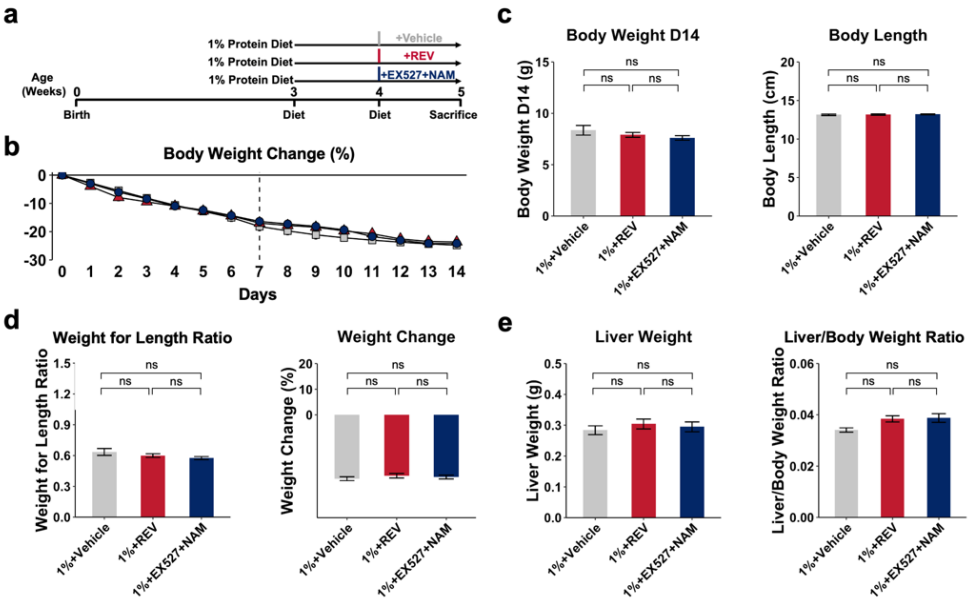

Fig. 6 The effect of SIRT1 modulators on basic animal characteristics. a Experiment design. **b** Body weight change throughout experiment (n=6). **c** Average food and liquid intake during day 7 to day 14 (n=6). **d** Final body weight, body length, and weight for length ratio assessed at day 14 (n=6). **e** Liver weight, liver weight to body weight ratio (n=6). $^{*}p < 0.05$, $^{**}p < 0.01$, $^{***}p < 0.001$, ns as not significant, one-way ANOVA followed by Tukey's post hoc test. Data are shown as the mean ± S.E.M.

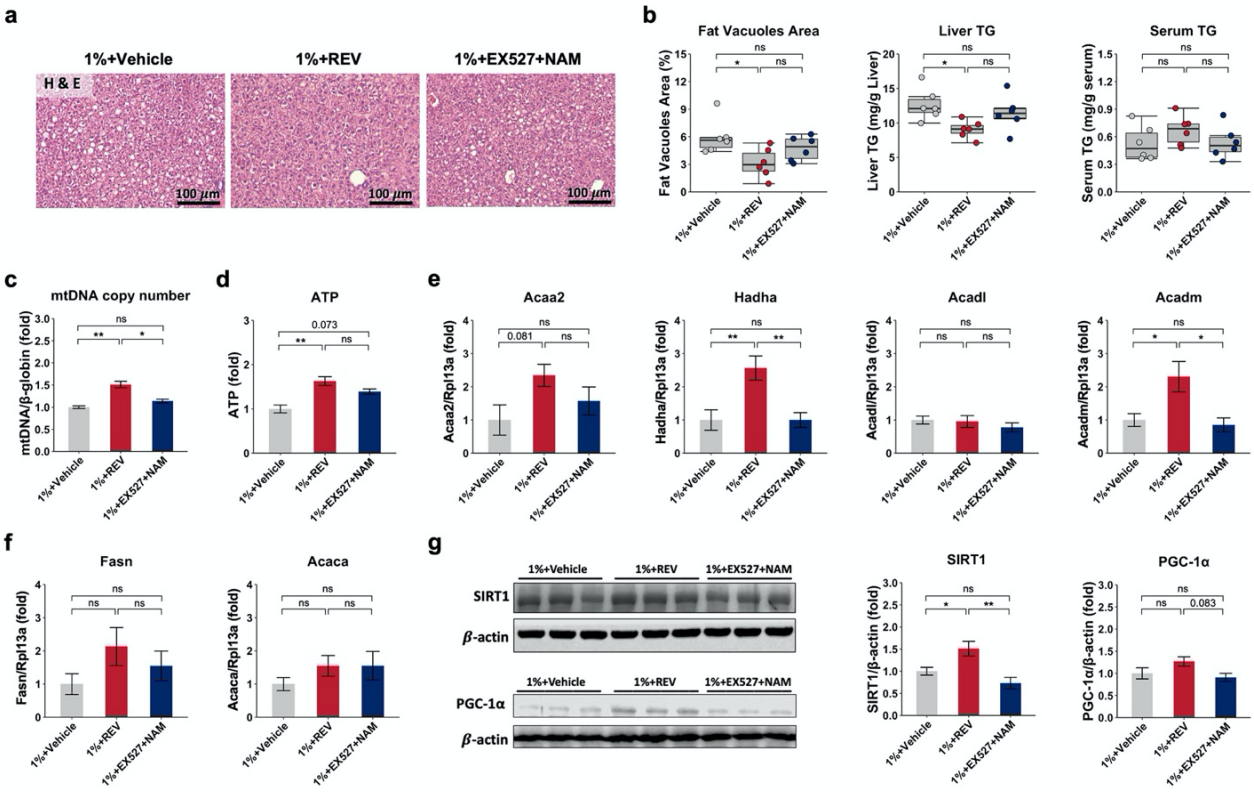

Fig. 7 The effect of SIRT1 modulators on hepatic steatosis, mitochondrial characteristics, SIRT1 and its downstream targets. a Representative hematoxylin and eosin staining images of the liver (20X magnification). Cytoplasm was stained in red, and nucleus was stained in purple. **b** Quantification of liver histology and TG levels (n=6). **c** mtDNA copy number (n=6). **d** ATP levels (n=6). **e** mRNA expression of β-oxidation genes (n=6). **f** mRNA expression of lipid genesis genes (n=6). **g** SIRT1 and PGC-1α western blots and quantification (n=3). $^{*}p < 0.05$, $^{**}p < 0.01$, $^{***}p < 0.001$, ns as not significant, one-way ANOVA followed by Tukey's post hoc test. Data are shown as the mean ± S.E.M. Scale bars are as indicated.

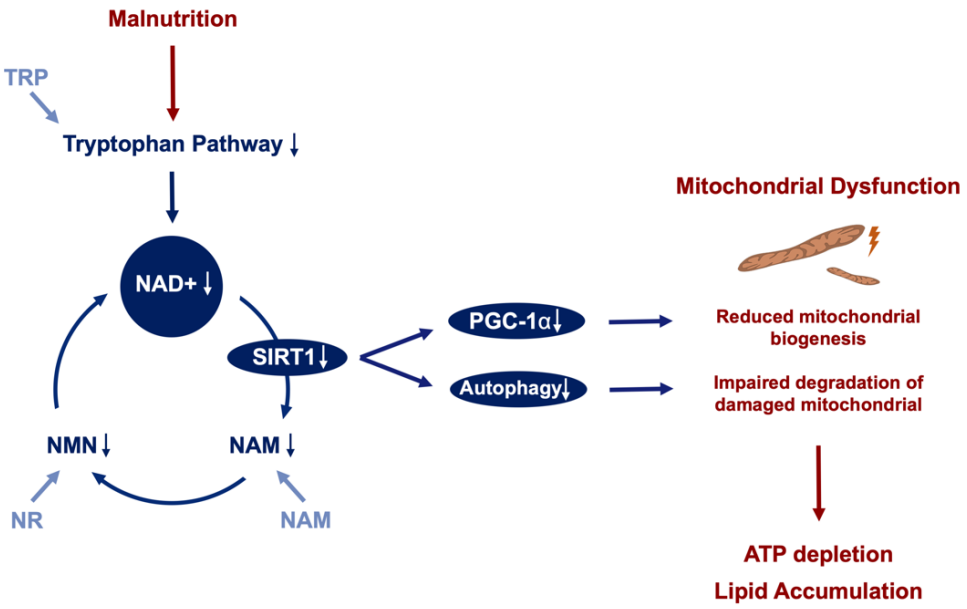

718

719 **Fig. 8 Proposed model of the role of the TRP-NAM pathway in malnutrition-induced hepatic**
720 **metabolic disturbances.** In protein malnutrition, decreased TRP availability will decrease the
721 kynurenine pathway activity, which is associated with NAD+ and NAM deficiency. This would
722 disturb NAD+ salvage pathway, including SIRT1, influence its downstream target PGC-1α and
723 autophagy, which affect mitochondrial quality and function. These changes lead to ATP depletion
724 and lipid accumulation in the liver. We hypothesize that supplement with TRP-NAM modulator
725 would influence NAD+ salvage pathway. This would thereby activate SIRT1, influence PGC-1α
726 deacetylation and autophagy, which will have a positive effect on mitochondrial health, affect
727 mitochondrial biogenesis and clearance of damaged mitochondrial, then improve ATP generation
728 and reduce lipid accumulation in the liver.